INVITED ARTICLE

TECHNOLOGY

Dextran functionalization enhances nanoparticle-mediated siRNA delivery and silencing

Daniel Vocelle[1], Olivia M. Chesniak[2], Amanda P. Malefyt[1], Georgina Comiskey[2], Kwasi Adu-Berchie[1], Milton R. Smith III[2], Christina Chan[1,3] & S. Patrick Walton[1]

Understanding the endocytosis and intracellular trafficking of short interfering RNA (siRNA) delivery vehicle complexes remains a critical bottleneck in designing siRNA delivery vehicles for highly active RNA interference (RNAi)-based therapeutics. In this study, we show that dextran functionalization of silica nanoparticles enhanced uptake and intracellular delivery of siRNAs in cultured cells. Using pharmacological inhibitors for endocytotic pathways, we determined that our complexes are endocytosed via a previously unreported mechanism for siRNA delivery in which dextran initiates scavenger receptor-mediated endocytosis through a clathrin/caveolin-independent process. Our findings suggest that siRNA delivery efficiency could be enhanced by incorporating dextran into existing delivery platforms to activate scavenger receptor activity across a variety of target cell types.

***Keywords*: Nanoparticles; siRNAs; Delivery Vehicles; Scavenger Receptors; Dextran; Clathrin; Caveolin; RNA Interference; RNAi; Silica; Endocytosis; Lung Carcinoma; H1299; Confocal Microscopy; HeLa.**

INNOVATION

It is common that siRNA delivery vehicles that are effective in cell culture studies fail *in vivo*[1]. This is often due to toxicity, immunogenicity and limited bioavailability when administered systemically. Overcoming these issues has been an area of considerable focus, with some successes. Unfortunately, for even the successful vehicles, delivery efficiencies remain low due to an incomplete understanding of the cellular and molecular mechanisms associated with cytoplasmic delivery of short interfering RNAs (siRNAs)[2]. Furthermore, it may be that the mechanisms that are necessary for functional siRNA delivery vary with the type of vehicle being used. Here, we describe our novel approach to improving the endocytosis and intracellular trafficking of delivery vehicles — inclusion of dextran in the particle synthesis. Improved endocytosis and trafficking subsequently result in improved silencing from the delivered siRNA cargo. As such, our studies provide foundational information that will inform the design of future delivery vehicles.

INTRODUCTION

New therapeutic approaches are continually needed for targeting disease-associated proteins. siRNA therapeutics are a potential approach capable of highly specific targeting of a wide range of proteins through the activation of RNA interference (RNAi)[3]. With the assistance of delivery vehicles, siRNAs are transported from the extracellular environment into the cytoplasms of eukaryotic cells. After processing by the RNAi pathway proteins[4–8], siRNAs guide degradation of target messenger RNAs (mRNAs) in a sequence-specific manner, resulting in a decrease in target protein levels. siRNA therapeutics are being developed for the treatment of cancers, genetic disorders, and infectious diseases[2]. While siRNA technology is well established in the laboratory environment, continued progress on the *in vivo* use of siRNAs will depend on the development of improved delivery vehicles.

Delivery vehicles are required to prevent degradation of siRNAs by serum nucleases, rapid filtration of siRNAs by the kidneys or siRNA-initiated immunogenic responses[9–11]. Moreover, if designed correctly, delivery vehicles can maximize delivery of the siRNAs to the target cells/tissues of interest[12]. Currently, lipoplexes (complexes of siRNA with lipids) and polyplexes (complexes of siRNAs with polymers) are the most prevalent among ongoing clinical trials with some *in vivo* successes[3,2,13–17]. However, most existing delivery vehicles cannot be used clinically due to *in vivo* toxicity, immunogenicity or inactivity[16,18–21]. One means to address these limitations is through functional modifications[22–24]. One modification, dextran, has demonstrated success in enhancing the activity of multiple delivery vehicles[14,25–28]. Functionally, dextran has been used to reduce toxicity, prevent opsonization and block non-specific binding[29–31]. Furthermore, functionalization with dextran polymers has been used for targeted delivery to various tissues[32–34].

While progress has been made on enhancing the systemic and extracellular trafficking of delivery vehicles, transfection efficiencies among delivery vehicles remain low relative to viral vectors, due in part to an incomplete understanding of siRNA–vehicle complex endocytosis and intracellular trafficking[2,35]. It remains unclear if RNAi is associated with a particular mechanism of endocytosis or if the mechanism of cytoplasmic delivery is specific to a certain cell type or delivery vehicle.

[1]Department of Chemical Engineering and Materials Science, [2]Department of Chemistry, [3]Department of Biochemistry and Molecular Biology, Michigan State University, East Lansing, MI 48824-1226, USA. Correspondence should be addressed to S.P.W. (spwalton@egr.msu.edu)

Received 18 August 2015; accepted 23 February 2016; published online 31 March 2016; doi:10.1142/S2339547816400100

Lipid- and polymer-based vehicles have been reported to use clathrin-mediated endocytosis, caveolae-mediated endocytosis, macropinocytosis and phagocytosis[36–38], though endocytosed material typically remains in endosomal compartments rather than entering the cytoplasm[35,39]. siRNAs unable to escape early endosomes are exocytosed or degraded[40]. It has been postulated that siRNAs and complexes escape the endosomes via lipid fusion with the membrane, endosomal swelling (proton sponge effect), leaky membranes or, for vehicles with the appropriate functional groups, photochemical disruption[39]. However, these escape mechanisms are not used in all cases[41,42]. Recent reports suggest that activation of RNAi may not even require endosomal escape[43], as the RNAi machinery has been found to be associated with early endosomes. Developing a better understanding of the intracellular trafficking events associated with RNAi remains a significant hurdle toward improving the efficacy of siRNA delivery vehicles.

The aim of this study was to investigate the impacts of chemical characteristics of delivery vehicles, specifically the inclusion of dextran, on influencing the endocytosis and intracellular trafficking of siRNA–silica nanoparticle (SNP) complexes. SNPs were chosen as a delivery platform for their highly tunable synthesis, consistent physical conformation, low cytotoxicity and delivery efficacy[17,44,45]. Our results showed that dextran significantly enhanced the utility of SNPs for delivering siRNAs to cultured cells, by initiating their uptake through a scavenger receptor-mediated endocytosis mechanism that is clathrin/caveolae-independent. Subsequent degradation of the SNPs, attributed in part to the acidic conditions of intracellular vesicles, suggested a means for activating release of the siRNAs from the SNPs and initiation of the silencing cascade.

METHODS

Materials

See **Supplementary Table 1** for a detailed list of reagents.

Cell culture

H1299 cells constitutively expressing a 2 hour half-life EGFP were generously provided by Dr. J. Kjems (University of Aarhus, Denmark). H1299 and HeLa cells were maintained in DMEM High Glucose, 10% fetal bovine serum, and 1% penicillin/streptomycin. 1% Geneticin was included in the H1299 culture medium to maintain EGFP expression. Cells were incubated at 37°C in 5% CO_2, at 100% relative humidity, and subcultured every 4–5 days by trypsinization.

Synthesis of silica nanoparticles

A 500 mL round bottom Schlenk flask was charged with 150 mL of absolute ethanol and 50 mL of Milli-Q water 18 MΩ with constant stirring. Dextran (9–11 kDa, 2.4×10^{-6} mol, 24 mg) was dissolved in 10 mL of Milli-Q water and added, followed by 10 mL of NH_4OH (~30% as NH_3). Tetraethyl orthosilicate (TEOS) (2.4 mmol, 0.53 mL) was added dropwise via syringe. The mixture was stirred for 10 minutes at room temperature (RT) under nitrogen followed by addition of (3-Aminopropyl) triethoxysilane (APTES) (concentration varied as mole percentage of TEOS; e.g., 40% APTES used 0.96 mmol, 0.224 mL). The reaction mixture was stirred for 24 hours at RT under nitrogen atmosphere and purified by pressure filtration using an Ultracel regenerated cellulose membrane (30 kDa MWCO) at 40 psi and rinsed three times with Milli-Q water. The filtered solids were suspended in Milli-Q water and sonicated until well dispersed.

Zeta potential

A Malvern Zetasizer Nano ZS was used to determine the zeta potential (mV) of SNPs. Measurements were collected using 1 mg/mL of SNP in HEPES buffer.

EGFP silencing analysis

H1299-EGFP cells were seeded in 96-well plates at a density of 200,000 cells/mL in 100 uL of growth media without antibiotics. Cells were treated 24 hours post-seeding with a 50 µL transfection solution containing Opti-MEM, siRNA and delivery vehicle that was mixed for 30 minutes prior to addition to the cells. Final concentrations were maintained at 100 nM siRNA in either 2.3 µg/mL Lipofectamine 2000 (LF2K) or 200 µg/mL SNP. Cells were incubated in the transfection solutions at 37°C, 5% CO_2 and 100% humidity. At 24 hours after transfection, cells were washed twice with Dulbecco's NaCl/Pi (DPBS), and EGFP fluorescence was quantified with a Gemini EM fluorescent plate reader (Molecular Devices) at 480 nm excitation and 525 nm emission. Fluorescence intensity was normalized to control wells treated with a delivery vehicle but no siRNA. Cytotoxicity was monitored by microscopy of cell morphology and EGFP expression and was not observed in any of the treatments (**Supplementary Fig. 1**).

HeLa cells were seeded in 96-well plates at a density of 100,000 cells/mL in 100 µL of antibiotic-free growth media. Cells were treated 24 hours post-seeding with a 50 µL transfection solution containing Opti-MEM, 20 ng pd2EGFP-N1 and 2.3 µg/mL LF2K. Cells were then treated with a 50 µL transfection solution containing Opti-MEM, siRNA and delivery vehicle that was mixed for 30 minutes prior to addition to the cells. Final concentrations were maintained at 100 nM siRNA in either 2.3 µg/mL LF2K or 200 µg/mL SNP. Cells were incubated in the transfection solutions at 37°C, 5% CO_2 and 100% humidity. Cells were washed 4 hours post-transfection with antibiotic free growth media. At 24 hours after transfection, cells were washed twice with DPBS, and EGFP fluorescence was quantified with a Gemini EM fluorescent plate at 480 nm excitation and 525 nm emission. Fluorescence intensity was normalized to control wells treated with a delivery vehicle but no siRNA (**Supplementary Fig. 2**). Cytotoxicity was monitored by microscopy of cell morphology and EGFP expression and was not observed in any of the treatments.

Inhibition experiments

EGFP-expressing H1299 cells were seeded in 12-well plates at a density of 150,000 cells/well and cultured in antibiotic free growth media. Immediately prior to transfection, cells were washed with media and replaced with inhibitor containing media for the appropriate pre-treatment time: chlorpromazine (10 µg/mL, 30 minutes), filipin complex III (2 ug/mL, 60 minutes), cytochalasin D (5 µg/mL, 15 minutes), temperature (4°C, 60 minutes) and 500 kDa dextran sulfate (200 µg/mL, 30 minutes). Following pre-treatment, cells were treated with 100 µL of various transfection solutions in Opti-MEM (200 nM siRNA and either 2.3 µg/mL LF2K or 200 µg/mL SNP) and incubated at 37°C, 5% CO_2 and 100% relative humidity. Cells were washed 4 hours post-transfection with media containing 20 µg/mL heparin for 15 minutes at 37°C to remove extracellularly bound complexes. Antibiotic-free media was then added to the cells.

For FACS analysis, cells were trypsinized 24 hours post-transfection, pelleted by centrifugation (200 *g*) at 4°C and re-suspended in DPBS. The cells were then transferred into 5 mL round bottom tubes. Immediately prior to analysis, cells were treated with DAPI at a final concentration of 1 µg/mL for live/dead analysis. Cells were analyzed using a Becton Dickinson Influx Flow Cytometer to detect DAPI (355/460), EGFP (488/530) and Dy547-tagged siRNA (561/585), gated to include 10,000 events/sample. For comparison across experiments, the instrument was calibrated using Sphero Rainbow Calibration particles. Geometric mean was used to calculate fluorescence intensity values among samples. EGFP fluorescence was normalized to particle only controls treated with the corresponding inhibitor. Dy547 fluorescence was normalized to the uptake of siRNA only (no vehicle) controls.

HeLa cells were seeded in 96-well plates in antibiotic-free growth media. Cells were transiently transfected 24 hours post-seeding with pd2EGFP-N1 and LF2K. Immediately prior to transfection, cells were washed with media and replaced with inhibitor containing media for the appropriate pre-treatment time and incubated at 37°C, 5% CO_2 and 100% humidity. Cells were washed 4 hours post-transfection with antibiotic free growth media. Cells were washed twice with DPBS

24 hours post-transfection, and EGFP fluorescence was quantified using a Gemini EM fluorescent plate reader at 480 nm excitation and 525 nm emission. Fluorescence intensity was normalized to control wells treated with a delivery vehicle but no siRNA (**Supplementary Fig. 2**). Cytotoxicity was monitored by microscopy of cell morphology and EGFP expression and was not observed in any of the treatments.

Transmission electron microscopy/energy dispersive X-ray spectroscopy

Intracellular transmission electron microscopy (TEM): EGFP-expressing H1299 cells were seeded in six-well plates at a density of 400,000 cells/well and cultured in antibiotic-free media. Cells were treated 24 hours post-seeding with 200 µL transfection solutions (Opti-MEM, 200 nM siRNA and 200 µg/mL SNP) and incubated at 37°C, 5% CO_2 and 100% relative humidity. Cells were trypsinized 24 hours post-transfection and pelleted by centrifugation (200 RCF) at 4°C. Samples were fixed using 2.5% formaldehyde/glutaraldehyde in DPBS, stained with 1% osmium tetroxide in DPBS, dehydrated through a graded series of ethanol concentrations and embedded in Spurr resin. Samples were sectioned to a thickness of ~90 nm using an RMC MYX ultramicrotome and placed onto a 200-mesh formvar coated copper grid. Samples were additionally stained with uranyl acetate and lead citrate. Images were acquired using a JEOL 100CXII transmission electron microscope operating at an accelerating voltage of 100 keV and equipped with an Olympus MegaView III digital camera. Energy dispersive X-ray spectroscopy (EDS) analysis was performed on JEOL 2200FS transmission electron microscope operating at an accelerating voltage of 200 keV.

Confocal microscopy

EGFP-expressing H1299 cells were seeded in 4-well plates at a density of 75,000 cells/well and cultured in antibiotic free growth media. Immediately prior to transfection, cells were washed with media and replaced with inhibitor-containing media for the appropriate pre-treatment time: chlorpromazine (10 µg/mL, 30 minutes), filipin complex III (2 µg/mL, 60 minutes), cytochalasin D (5 µg/mL, 15 minutes) and 500 kDa dextran sulfate (200 µg/mL, 30 minutes). Following pre-treatment, cells were treated with 100 µL of various transfection solutions in Opti-MEM (200 nM siRNA and either 2.3 µg/mL LF2K or 200 µg/mL SNP) and incubated at 37°C, 5% CO_2 and 100% relative humidity. Cells were washed 4 hours post-transfection with Opti-MEM to remove extracellularly bound complexes and imaged 4 hours and 24 hours post-transfection (**Supplementary Fig. 3,4**).

Confocal images were taken using an Olympus FluoView 1000 spectral-based laser scanning confocal microscope. An Olympus PLAPON 60×/1.42 oil objective was used to acquire all images. EGFP (488/530) fluorescence was measured using an excitation of 488 nm with a multi-line Argon laser, and displayed as green (LUT). Dy547 (559/568) fluorescence (siRNA) was excited at 559 nm by a HeNe laser, and displayed as red (LUT). The focal plane for each image was chosen based on the highest intensity EGFP fluorescence. All images were collected sequentially as single XY images and used two-count Line Kalman averaging.

Acidic degradation

SNPs were dispersed in acetic acid (pH 4.75) at a concentration of 0.5 mg/ml and incubated at RT. After 16 hours, the samples were centrifuged and washed three times with DPBS. Samples were prepared for imaging by placing 5 µL of the sample onto a 200-mesh formvar coated copper grid and air dried overnight. Images were acquired using a JEOL 100CXII transmission electron microscope operating at an accelerating voltage of 100 keV and equipped with an Olympus MegaView III digital camera.

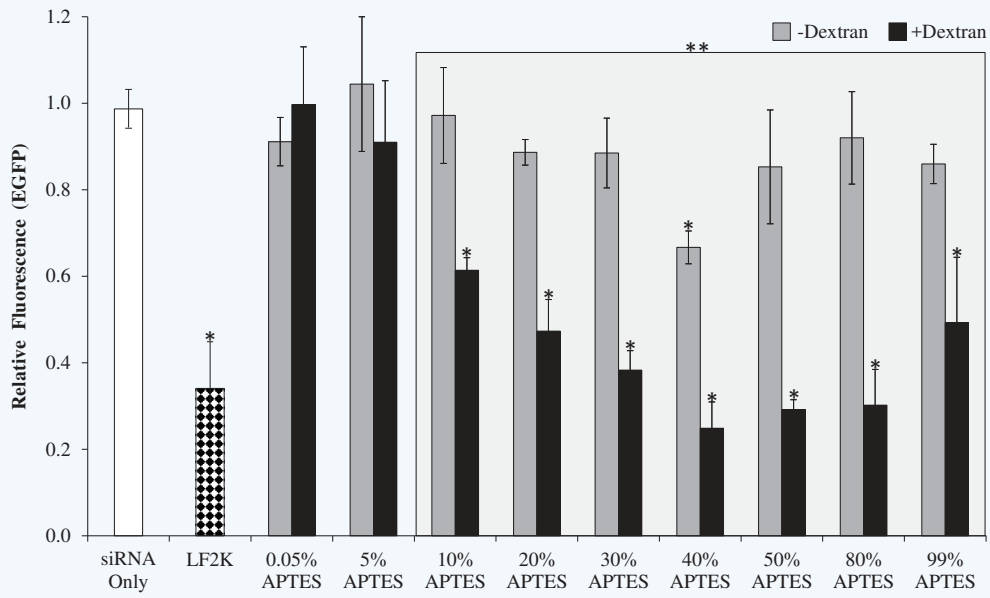

Figure 1 Effect of dextran and amine content on silencing. Relative fluorescence of EGFP-expressing H1299 cells transfected for 24 hours with siRNA complexes and normalized to the EGFP fluorescence of vehicle-only control cells. The complexes contain either 2.3 µg/mL of LF2K or 200 µg/ml of SNPs functionalized with varying percentages of APTES and either 0 mol% (hatched) or 1 mol% dextran (filled), and 100 nM of siRNA. Error bars represent ±1 standard deviation; $n = 3$. Statistical analysis was performed using two-way ANOVA, followed by Tukey's HSD post-hoc analysis. *Significant difference ($p < 0.05$) as compared to vector-only treatments. **Significant difference ($p < 0.05$) of non-dextran SNPs to dextran-containing SNPs.

Polyacrylamide binding gels

Solutions were prepared in DPBS, using 200 nM siRNA, and 200 µg/mL SNP, and allowed to incubate for 30 minutes. Milli-Q water (pH 7.00, control) or acetic acid (pH 4.75) was added to the sample and incubated at RT. After 16 hours, the samples were centrifuged to pellet the SNPs, washed with Milli-Q water and suspended in DPBS. Each sample was mixed with 300 µg/mL heparin (Sigma) for 3 minutes to elute the siRNA from the SNPs and then resolved on a 12% polyacrylamide gel. In lieu of centrifugation and washing, siRNA samples without SNP were diluted with Milli-Q water. Nucleic acid detection was performed with SYBR gold staining, imaging was performed with the Molecular Imager ChemiDoc XRS System, and analysis was performed using ImageJ[46].

Statistical analyses

Multiple comparisons were performed with two-way ANOVA followed by Tukey's HSD post hoc

Table 1 Target and mechanism of action for endocytosis inhibitors[37,47].

Inhibitor	Target	Mechanism of action
Chlorpromazine	Clathrin-mediated endocytosis	Inhibits formation of clathrin coated pits
Filipin	Caveolae-mediated endocytosis	Removes cholesterol from caveolae
Cytochalasin D	Actin dependent processes	Depolymerizes actin and disrupts actin filament formation
Temperature	Energy dependent processes	Reduces membrane fluidity and available ATP
Dextran Sulfate	Scavenger receptors	Competitive inhibitor for acetyl-LDL receptors

analysis (**Supplementary Tables 2–4**). Analyses were performed using OriginPro 8 and Microsoft Excel.

RESULTS

Effect of amine and dextran content on siRNA silencing efficiency

SNPs were synthesized with varying concentrations of the primary amine-containing moiety APTES, with and without dextran, to determine if these variables (amine content and the presence of dextran) influenced the delivery or silencing of the siRNA cargo (**Fig. 1**). At 24 hours post-transfection, seven of the nine dextran-containing SNPs achieved significant silencing compared to the nanoparticle only controls. Six achieved >50% reduction in EGFP levels and were statistically equivalent to LF2K. Increasing amines resulted in increased silencing, with maximal silencing achieved at 40% APTES, with little gain and perhaps some loss of activity at higher amine contents. Only one non-dextran SNP achieved statistically significant reduction in EGFP levels, again at 40% APTES. SNPs were characterized for their potential to bind siRNA using zeta potential (**Supplementary Fig. 5**). Both the silencing data (~40% APTES) and ζ potential (~27 mV) results suggest that there may be an ideal amine content/charge density for siRNA delivery vehicles, though further characterization would be required to establish this concretely. As our objective was to understand better the uptake and trafficking mechanism for SNPs that yield active silencing, we focused our subsequent analyses on our best performing SNP (40% APTES with dextran).

Inhibition of siRNA endocytosis and silencing

Having confirmed the ability of our SNPs to deliver siRNAs that then silence the EGFP target, we wished to evaluate the mechanism of uptake for our SNP–siRNA complexes as compared to LF2K lipoplexes and naked siRNAs. From the literature, we selected a number of chemical inhibitors for individual endocytosis pathways (**Table 1**) and investigated the quantity of siRNA delivered (**Fig. 2**) and the silencing achieved (**Fig. 3**) following delivery of siRNAs using our most effective SNP (40% APTES + Dextran), LF2K or no vehicle.

As expected, intracellular levels of siRNA were significantly increased using LF2K (5× increase) and SNPs (40× increase), compared to naked siRNA (**Fig. 2**, see insets). Delivery by LF2K was significantly reduced by the combination of chlorpromazine and filipin, low temperature (4°C) and dextran sulfate. For SNP delivery, the active inhibitors were chlorpromazine, cytochalasin D, low temperature (4°C) and dextran sulfate. The differential effects of the inhibitors indicate that the SNPs were endocytosed through a mechanism distinct from that

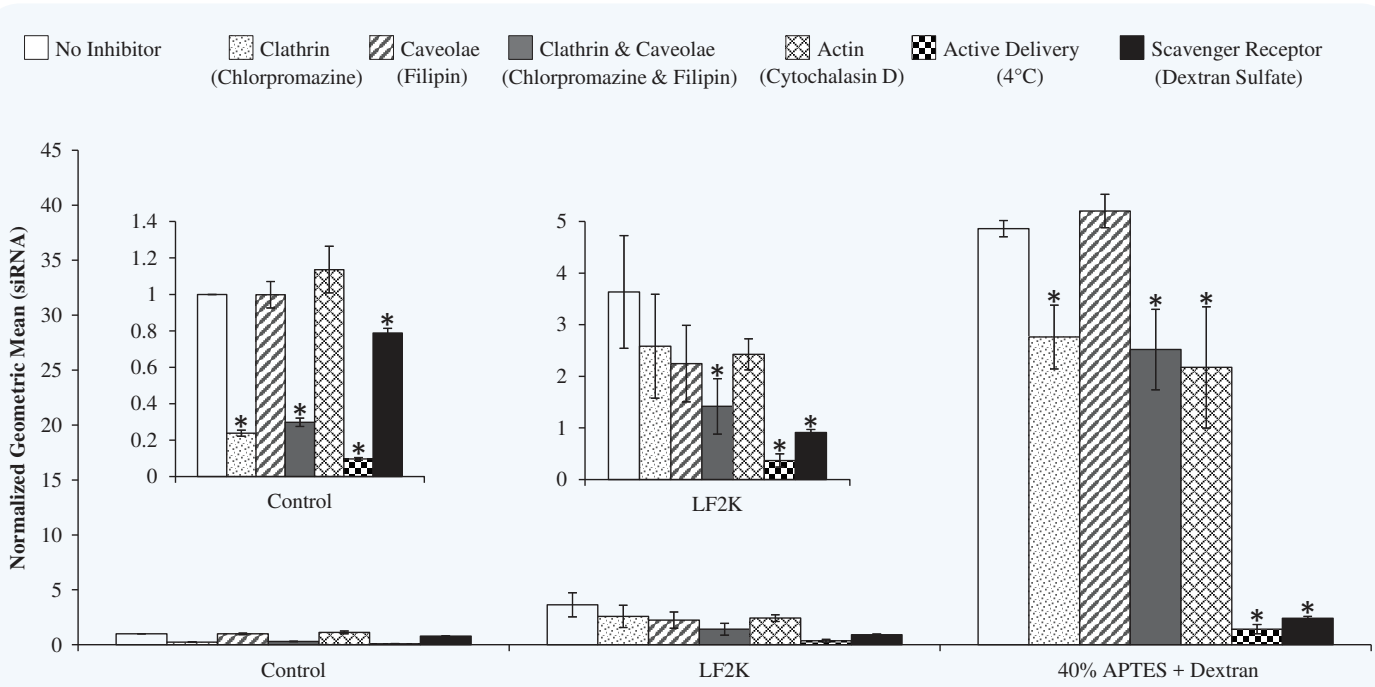

Figure 2 Influence of endocytotic inhibitors on the uptake of siRNA. Relative fluorescence of complexes containing an EGFP-targeting, fluorescently-labeled siRNA delivered to EGFP expressing H1299 cells. Cells were pre-treated with endocytosis inhibitors and assayed 24 hours post-transfection using flow cytometry. Results are normalized to uptake of siRNA only controls. Error bars represent ±1 standard deviation; $n = 3$. Statistical analysis was performed using two-way ANOVA, followed by Tukey's HSD post-hoc analysis. *Significant difference ($p < 0.05$) as compared to delivery in the absence of inhibitor.

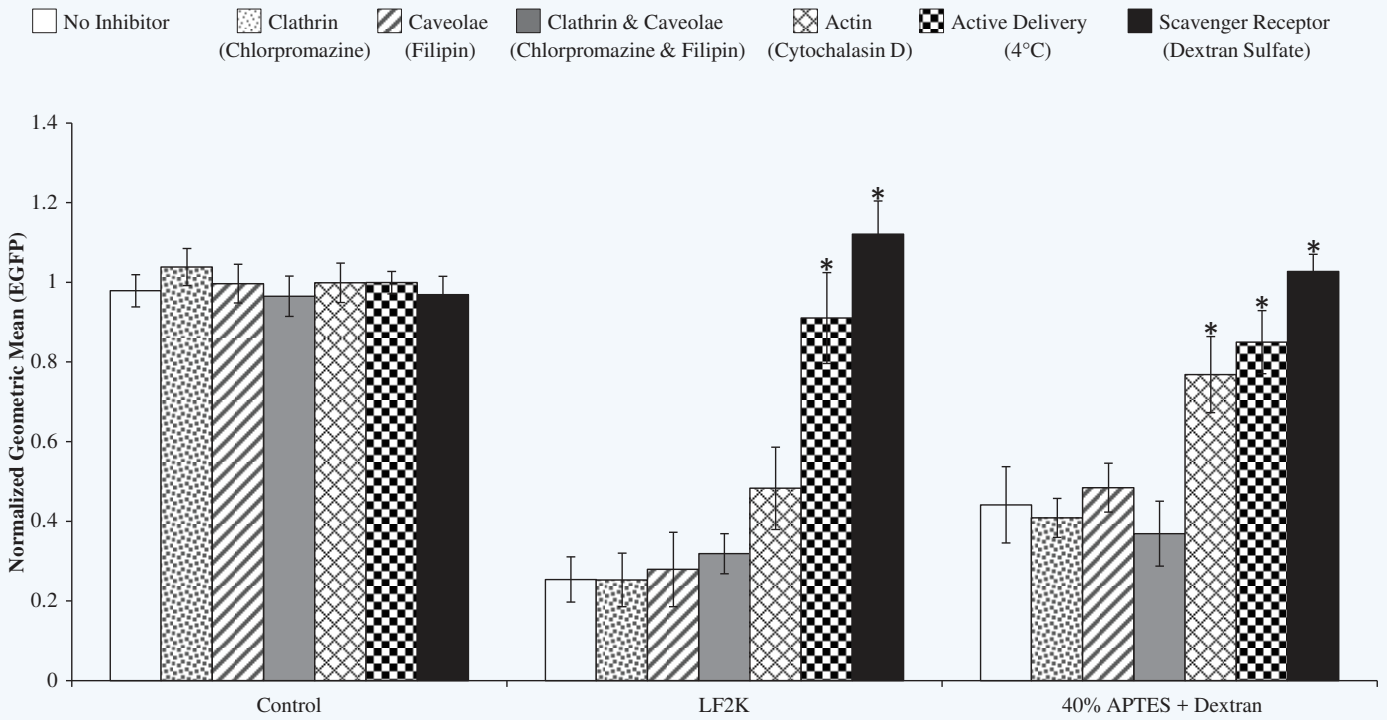

Figure 3 EGFP silencing in the presence of endocytotic inhibitors. Relative EGFP fluorescence in EGFP-expressing H1299 cells after delivery of complexes containing an EGFP-targeting, fluorescently-labeled siRNA. Cells were pre-treated with endocytosis inhibitors and assayed 24 hours post-transfection in flow cytometry. Results were normalized to particle only controls within corresponding inhibitor. Error bars represent ±1 standard deviation; $n = 3$. Statistical analysis was performed using two-way ANOVA, followed by Tukey's HSD post-hoc analysis. *Significant difference ($p < 0.05$) as compared to conditions without inhibitors.

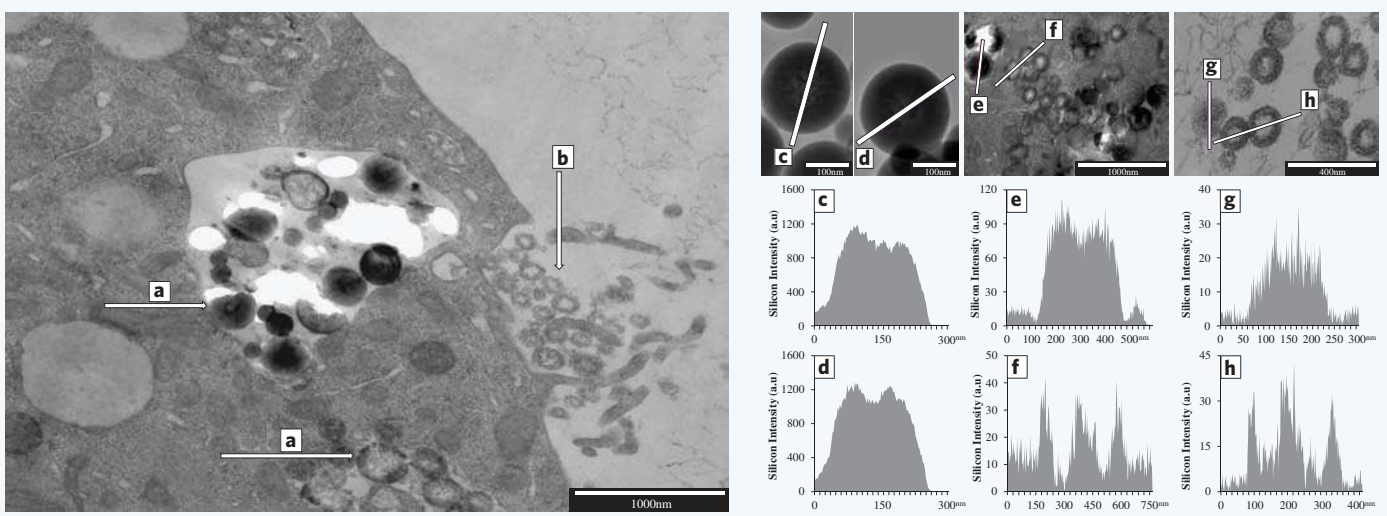

Figure 4 TEM analysis of SNP-siRNA complex endocytosis and trafficking. TEM images show internalization of SNPs (40% APTES + Dextran) within EGFP-expressing H1299 cells 24 hours post-transfection. (**a**) Intracellular SNPs are contained in vesicles and show varying degrees of degradation. (**b**) SNPs with internal degradation are observed in the extracellular environment. EDS line scan analysis for silicon on non-transfected (**c,d**), intracellular (**e,f**), and extracellular (**g,h**) particles.

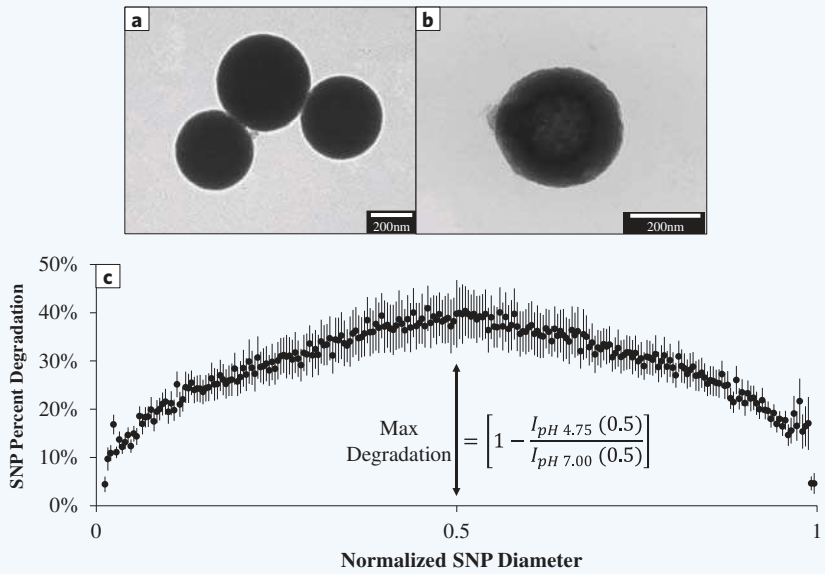

Figure 5 SNP degradation under acidic conditions. Relative intensity (I) of SNPs (40% APTES + Dextran) exposed to neutral or acidic conditions. SNPs were suspended in a (**a**) pH 7.00 or (**b**) pH 4.75 solution for 16 hours at RT and imaged using TEM. (**c**) Percent degradation was determined by comparing the difference in relative intensity at pH 4.75 to that at pH 7.00, using a normalized particle diameter. Average diameter of pre-acid particles was 381 nm ± 32 nm; after acid, the average diameter was 375 nm ± 28 nm. Error bars represent ±1 standard deviation; $n = 10$. Scale bars are 200 nm.

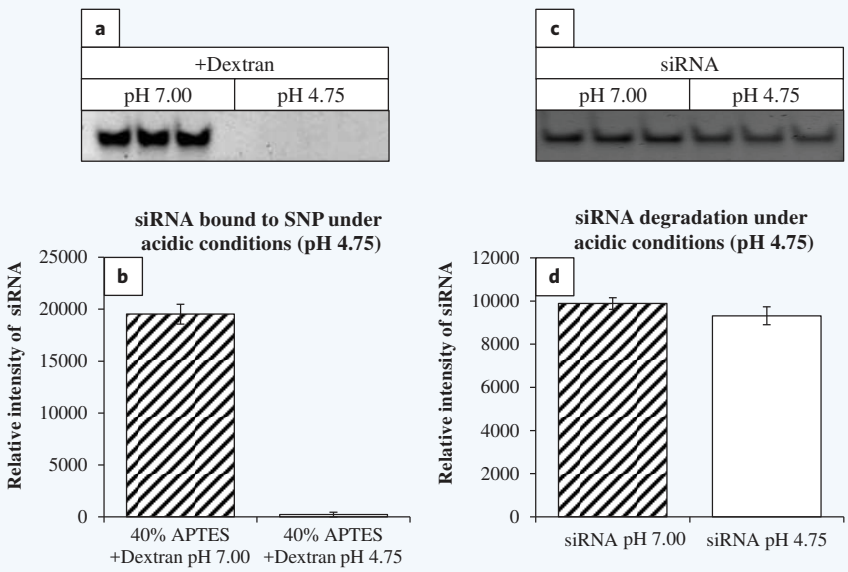

Figure 6 Nucleic acid release under acidic conditions. Relative intensity of siRNA exposed to acidic conditions (pH 4.75). (**a**,**b**) Complexes were prepared in DPBS (200 nM siRNA and 200 µg/ml SNP 40% APTES + Dextran) and then incubated for 16 hours at RT in an acidic solution (pH 4.75). Results are normalized to siRNA release at pH 7.00. (**c**,**d**) siRNA (200 nM) was incubated for 16 hours in an acidic solution (pH 4.75) without delivery vehicles. Results are normalized to siRNA exposed to pH 7.00. Error bars represent ±1 standard deviation; $n = 3$. Statistical analysis was performed using one-way ANOVA, followed by Tukey's HSD post-hoc analysis. A significant difference ($p < 0.05$) between acidic and neutral conditions was found for siRNA binding (**a**,**b**) but not degradation (**c**,**d**).

of LF2K. Moreover, plasmid DNA delivered with our SNPs (**Supplementary Fig. 6**) did not result in significant overexpression whereas plasmid delivery with LF2K resulted in significant gene overexpression, further suggesting that SNPs and LF2K deliver through different pathways. However, the strong impact of dextran sulfate suggests that both SNP and LF2K complexes used scavenger receptor-mediated uptake in delivering siRNAs. Our FACS analyses were corroborated using confocal microscopy at 4 hours and 24 hours after transfection (**Supplementary Fig. 3,4**). Likewise, to examine the generality of our results across cell types, replicate experiments were performed in HeLa cells, producing similar results (**Supplementary Fig. 2**).

In examining the resulting silencing in the presence of inhibitors (**Fig. 3**), low temperature and dextran sulfate significantly reduced silencing following delivery by both LF2K and our SNP. This is a direct reflection of the inhibition observed for siRNA delivery (**Fig. 2**). This suggests that both SNP–siRNA complexes and LF2K–siRNA lipoplexes are effectively endocytosed and processed by the scavenger receptor pathway. However, there are discrepancies between the inhibition of delivery and the reduction in silencing activity. Cytochalasin D also significantly inhibited silencing by SNP delivery, indicating that the processing of endocytotic vesicles on actin networks may be essential for silencing, regardless of the pathway of endocytosis.

Intracellular trafficking of SNPs

Using TEM, we confirmed the uptake of our SNP-siRNA complexes and identified the subcellular locations to which SNPs were trafficked (**Fig. 4**). In all cases, we confirmed the presence of our SNPs using EDS line scans to detect silicon, which should not be present at significant levels endogenously (**Fig. 4c–f**). The images showed SNPs localized within membrane-bound endocytotic vesicles. Visual inspection of the signal intensity for the endocytosed particles suggested that the density of the interiors of the particles was decreased relative to particles before endocytosis. This observation was further supported by the appearance of degraded SNPs adjacent to the cell membrane, suggesting that these have been recently exocytosed from the cells.

Acidic degradation of SNPs

To determine if the observed intracellular degradation of our SNPs could be attributed to the acidic environments of some vesicles, we tested whether acidic pH would result in similar degradation patterns *in vitro* (**Fig. 5**). Both visual inspection (compare signal intensities for **Fig. 5a,b**) and quantification of the signals from multiple treated and untreated particles (**Fig. 5c**) indicate that acidic conditions promote SNP degradation with maximum degradation, roughly 40% of the TEM signal, in the centers of the particles. The particles appear rough after exposure to acid, again reflecting what was observed in the cellular experiments, suggesting some surface degradation. However, the

average diameter of the particles did not change significantly during the *in vitro* acid exposure.

siRNA binding under acidic conditions

We hypothesized that the degradation of the SNPs would contribute to the release of siRNAs from the complexes, resulting in a more rapid activation of silencing than would be achieved by purely diffusive release. To examine whether acidic conditions promoted nucleic acid release from SNPs, we incubated complexes of SNPs with siRNAs under neutral and acidic conditions. The amount of nucleic acid retained on the particles after exposure to acid was assayed using gel electrophoresis. Acidic conditions resulted in only 4% of the original nucleic acid being retained in complexes with the SNPs (**Fig. 6a,b**). The relatively minimal degradation of the naked nucleic acids in acid suggested that the reduction in retained material was not due to degradation of the nucleic acids but a reduced ability of the particles to bind them (**Fig. 6c,d**).

DISCUSSION

Designing effective, non-toxic siRNA delivery vehicles remains a critical challenge in the development of siRNA therapeutics. Here, we used SNPs as a means of identifying chemical characteristics of delivery vehicles that correlate with high activity of the delivered siRNA cargo. The SNP system is convenient as it allows for changes in the chemical functionality of the vehicle without altering its physical conformation. We plan to use the SNP system as a platform for further evaluation of other chemical functionalities (e.g., biodegradable disulfide linkages, PEGylation) that may enable high activity of the delivered siRNAs, with the goal of identifying characteristics that apply to any siRNA delivery vehicle. Moreover, by modifying the synthesis protocol, we will also be able to examine these characteristics on particles of multiple sizes. Our approach differs from purely combinatorial efforts that have been undertaken[48], where both the chemical functionality and the molecular structure/size of the vehicle can change simultaneously, potentially confounding why some vehicles result in higher siRNA activity than others.

Our data suggest that the majority of silencing that occurs results from uptake of either LF2K lipoplexes or SNP–siRNA complexes through a clathrin/caveolae-independent, energy-dependent process mediated by scavenger receptors. While nucleic acids and gold nanoparticles have been shown to be taken up via scavenger receptor-mediated endocytosis[49,50], this uptake mechanism was limited to macrophages and was either clathrin- or caveolae-dependent. Utilization of a clathrin/caveolae-independent, scavenger receptor-mediated pathway in non-macrophage cells distinguishes this mechanism of uptake from those previously reported.

For both vehicles, there were cases where changes in siRNA uptake and silencing were not correlated. For LF2K, where uptake inhibition by chlorpromazine and filipin did not result in a reduction in silencing, this may be because the amount of reduction in siRNA levels was small despite it being statistically significant. Additionally, it has been shown that lipoplexes enter cells through multiple pathways[51,52], making the inhibition of any one or two pathways, especially if those are not primary pathways to silencing, less likely to affect silencing.

For SNPs, the results are more complex. Inhibition by chlorpromazine, either in the presence or absence of filipin, resulted in a significant reduction in uptake with no concomitant reduction in silencing. This suggests inhibition of a non-productive uptake pathway. In contrast, cytochalasin D resulted in comparable levels of inhibition of siRNA uptake and a significant reduction in silencing. This indicates that SNP–siRNA complexes associate with the actin network, either directly or while in vesicles, and that this association is essential for delivering siRNAs in a manner (e.g., to a specific subcellular location) that eventually results in silencing. It is also worth noting that uptake, trafficking, and silencing are dynamic processes, and measurements at a single time point do not necessarily reflect a steady-state.

It is important to note that our SNPs deliver considerably more siRNA to cells than LF2K (~eight-fold, **Fig. 2**). This indicates that our SNPs deliver more siRNA than many delivery vehicles (using LF2K delivery as a reference)[53–55]. However, the degree of silencing achieved by the delivered siRNAs was only comparable to LF2K. This may indicate that a large fraction of the siRNAs delivered by SNPs is inactive due to sequestration, either by being retained on the SNPs or by being trapped in vesicles.[51] These internalized siRNAs may then be degraded prior to achieving silencing, mitigating any improvement in function that would result from delivery of higher quantities of siRNA. If this is the case, our SNPs may be valuable for delivering chemically modified siRNAs, in particular those designed for resistance to nucleases or enhanced endosomal escape, potentially providing a facile approach for increasing or extending the persistence of maximal silencing.[56]

Among the various classes of scavenger receptors, dextran sulfate is a known inhibitor of acetyl-LDL scavenger receptors, which are found among class A (SCARA1/SR-AI/II, SCARA2/MARCO) and class H (FEEL 1/stabilin-1/CLEVER-1, FEEL-2/stabilin-2/HARE)[57,58]. These receptors recognize targets with a high density of negative charges, common among bacterial polysaccharides[57]. While previously considered to be macrophage specific, scavenger receptors have been identified across multiple cell types including endothelial, smooth muscle, dendritic, fibroblast and epithelial cells.[58] Scavenger receptors are known to induce phagocytosis and macropinocytosis, although the exact signaling mechanism remains unknown.[59] Scavenger receptors can enact a variety of functional responses due to their association with various co-receptors (SRC family kinases, Toll-like receptors, β-integrins and tetraspanins)[59]. Our results suggest that the scavenger receptors used by our SNPs may associate with dynamin-independent GTPases of the Rho family, given their association with other scavenger receptors that had a reported role in actin polymerization and clathrin/caveolae-independent endocytosis.[60]

While the trafficking of high amine-content particles such as our SNPs within acidic endosomes suggests that siRNA release into the cytoplasm is due to the proton sponge effect[61], our results do not support this mechanism for endosomal release. From our TEM images, SNPs were only observed within membrane-bound vesicles and never observed in the nucleus or cytoplasm. These observations, in concert with the inability of SNPs to deliver plasmid DNA, are inconsistent with release mechanisms that require the endosomal membrane to rupture. Rather, it seems that only the siRNAs escape the endosomes in our system and that escape occurs after the SNP–siRNA complex has dissociated. This is further substantiated by our findings that acidic conditions inhibit the binding of siRNAs to SNPs. Formation of endosomal membrane pores would enable siRNA release into the cytoplasm. However, our SNPs lack any specific functionality designed to generate pores[62], making this unlikely. It may also be that siRNAs do not need to escape the endosomes to activate RNAi. Recent evidence has shown that RNAi pathway proteins, specifically Dicer and Ago2, are associated with vesicle and ER membranes[43,63]. It is possible that siRNAs are recognized in the endosomes after release from the SNPs, with the RNAi proteins able to shuttle them across the endosomal membrane. Based on our current results, however, the exact mechanism by which siRNAs achieve endosomal escape and initiate silencing remains unclear.

The design of siRNA delivery vehicles remains a somewhat haphazard process, without clear rules for which chemical and physical features provide the greatest probability of high siRNA activity. In this work, we have demonstrated that dextran associates with scavenger receptors to initiate clathrin/caveolae-independent endocytosis, and that internalization by this pathway results in active siRNA delivery. In doing so, we have identified both a vehicle design variable (presence of dextran)

and a biological mechanism (clathrin/caveolae-independent, scavenger receptor-mediated endocytosis) that warrant further examination for their contributions to the high activity of delivered siRNAs. Going forward, we hope to examine the generality of these rules for siRNA delivery vehicles based on lipids, polymers and nanoparticles.

ACKNOWLEDGEMENTS

We would like to thank the members of the Cellular and Biomolecular Laboratory (http://www.egr.msu.edu/cbl/) for their advice and support especially Stephen Lindeman, Sean Kappes and Sean Norton, for their assistance with this work. We thank the Michigan State University Center for Advanced Microscopy for their assistance: Dr. Alicia Withrow (biological TEM), Dr. Xudong Fan (physical TEM) and Dr. Melinda Frame (confocal). We would also like to express our gratitude for Dr. Louis King and his support in flow cytometry. We would also like to acknowledge the contributions of the late Professor Greg Baker to this work. Financial support for this work was provided in part by Michigan State University, the National Science Foundation (CBET 0941055, 1510895, 1547518) and the National Institutes of Health (GM079688, RR024439, GM089866, CA176854, DK081768, DK088251).

REFERENCES

1. Whitehead, K.A. *et al. In-vitro–in-vivo* translation of lipid nanoparticles for hepatocellular siRNA delivery. *ACS Nano* **6**, 6922–6929 (2012).
2. Yin, H. *et al.* Non-viral vectors for gene-based therapy. *Nat. Rev. Genet.* **15**, 541–555 (2014).
3. Burnett, J.C. & Rossi, J.J. RNA-based therapeutics: Current progress and future prospects. *Chem. Biol.* **19**, 60–71 (2012).
4. Sakurai, K. *et al.* A role for human Dicer in pre-RISC loading of siRNAs. *Nucleic Acids Res.* **39**, 1510–1525 (2011).
5. Tomari, Y. A protein sensor for siRNA asymmetry. *Science* **306**, 1377–1380 (2004).
6. MacRae, I.J., Ma, E., Zhou, M., Robinson, C.V. & Doudna, J.A. *In-vitro* reconstitution of the human RISC-loading complex. *Proc. Natl. Acad. Sci. U.S.A.* **105**, 512–517 (2008).
7. Gredell, J.A., Dittmer, M.J., Wu, M., Chan, C. & Walton, S.P. Recognition of siRNA asymmetry by TAR RNA binding protein. *Biochemistry* **49**, 3148–3155 (2010).
8. Noland, C.L., Ma, E. & Doudna, J.A. siRNA repositioning for guide strand selection by human Dicer complexes. *Mol. Cell* **43**, 110–121 (2011).
9. Whitehead, K.A., Dahlman, J.E., Langer, R.S. & Anderson, D.G. Silencing or stimulation? siRNA delivery and the immune system. *Annu. Rev. Chem. Biomol. Eng.* **2**, 77–96 (2011).
10. Layzer, J.M. *et al. In-vivo* activity of nuclease-resistant siRNAs. *RNA* **10**, 766–771 (2004).
11. Huang, Y. *et al.* Elimination pathways of systemically delivered siRNA. *Mol. Ther.* **19**, 381–385 (2011).
12. Angart, P., Vocelle, D., Chan, C. & Walton, S.P. Design of siRNA therapeutics from the molecular scale. *Pharmaceuticals* **6**, 440–468 (2013).
13. Kanasty, R., Dorkin, J.R., Vegas, A. & Anderson, D. Delivery materials for siRNA therapeutics. *Nat. Mater.* **12**, 967–977 (2013).
14. Davis, M.E. The first targeted delivery of siRNA in humans via a nanoparticle: From concept to clinic. *Mol. Pharm.* **6**, 659–668 (2009).
15. Burnett, J.C., Rossi, J.J. & Tiemann, K. Current progress of siRNA/shRNA therapeutics in clinical trials. *Biotechnol. J.* **6**, 1130–1146 (2011).
16. Knudsen, K.B. *et al. In-vivo* toxicity of cationic micelles and liposomes. *Nanomed. Nanotechnol. Biol. Med.* **11**, 467–477 (2015).
17. Asefa, T. & Tao, Z. Biocompatibility of mesoporous silica nanoparticles. *Chem. Res. Toxicol.* **25**, 2265–2284 (2012).
18. Mutlu, G.M. *et al.* Biocompatible nanoscale dispersion of single-walled carbon nanotubes minimizes *in-vivo* pulmonary toxicity. *Nano Lett.* **10**, 1664–1670 (2010).
19. Khlebtsov, N. & Dykman, L. Biodistribution and toxicity of engineered gold nanoparticles: A review of *in-vitro* and *in-vivo* studies. *Chem. Soc. Rev.* **40**, 1647–1671 (2011).
20. Moghimi, S.M., Hunter, A.C. & Andresen, T.L. Factors controlling nanoparticle pharmacokinetics: An integrated analysis and perspective. *Annu. Rev. Pharmacol. Toxicol.* **52**, 481–503 (2012).
21. Fadeel, B. & Garcia-Bennett, A.E. Better safe than sorry: Understanding the toxicological properties of inorganic nanoparticles manufactured for biomedical applications. *Adv. Drug Deliv. Rev.* **62**, 362–374 (2010).
22. Barros, S.A. & Gollob, J.A. Safety profile of RNAi nanomedicines. *Adv. Drug Deliv. Rev.* **64**, 1730–1737 (2012).
23. Moros, M. *et al.* Monosaccharides versus PEG-functionalized NPs: Influence in the cellular uptake. *ACS Nano* **6**, 1565–1577 (2012).
24. Gosnell, H. *et al.* Polymer-enhanced delivery increases adenoviral gene expression in an orthotopic model of bladder cancer. *J. Control. Release* **176**, 35–43 (2014).
25. Zhang, H., Ma, Y. & Sun, X.-L. Recent developments in carbohydrate-decorated targeted drug/gene delivery. *Med. Res. Rev.* **30**, 270–289 (2009).
26. Prijic, S. & Sersa, G. Magnetic nanoparticles as targeted delivery systems in oncology. *Radiol. Oncol.* **45**, 1–16 (2011).
27. Kim, J.S., Oh, M.H., Park, J.Y., Park, T.G. & Nam, Y.S. Protein-resistant, reductively dissociable polyplexes for *in-vivo* systemic delivery and tumor-targeting of siRNA. *Biomaterials* **34**, 2370–2379 (2013).
28. Ulery, B.D., Nair, L.S. & Laurencin, C.T. Biomedical applications of biodegradable polymers. *J. Polym. Sci. Part B Polym. Phys.* **49**, 832–864 (2011).
29. Passirani, C., Barratt, G., Devissaguet, J.P. & Labarre, D. Interactions of nanoparticles bearing heparin or dextran covalently bound to poly(methyl methacrylate) with the complement system. *Life Sci.* **62**, 775–785 (1998).
30. Rouzes, C., Gref, R., Leonard, M., De Sousa Delgado, A. & Dellacherie, E. Surface modification of poly(lactic acid) nanospheres using hydrophobically modified dextrans as stabilizers in an o/w emulsion/evaporation technique. *J. Biomed. Mater. Res.* **50**, 557–565 (2000).
31. Coombes, A.G.A. *et al.* Biodegradable polymeric microparticles for drug delivery and vaccine formulation: The surface attachment of hydrophilic species using the concept of poly(ethylene glycol) anchoring segments. *Biomaterials* **18**, 1153–1161 (1997).
32. Letourneur, D., Parisel, C., Prigent-Richard, S. & Cansell, M. Interactions of functionalized dextran-coated liposomes with vascular smooth muscle cells. *J. Control. Release* **65**, 83–91 (2000).
33. Cansell, M., Parisel, C., Jozefonvicz, J. & Letourneur, D. Liposomes coated with chemically modified dextran interact with human endothelial cells. *J. Biomed. Mater. Res.* **44**, 140–148 (1999).
34. Enochs, W.S., Harsh, G., Hochberg, F. & Weissleder, R. Improved delineation of human brain tumors on MR images using a long-circulating, superparamagnetic iron oxide agent. *J. Magn. Reson. Imaging* **9**, 228–232 (1999).
35. Ma, D. Enhancing endosomal escape for nanoparticle mediated siRNA delivery. *Nanoscale* **6**, 6415 (2014).
36. Rejman, J., Bragonzi, A. & Conese, M. Role of clathrin- and caveolae-mediated endocytosis in gene transfer mediated by lipo- and polyplexes. *Mol. Ther.* **12**, 468–474 (2005).
37. Malefyt, A.P., Walton, S.P. & Chan, C. Endocytosis pathways for nucleic acid therapeutics. *Nano LIFE* **02**, 1241005 (2012).
38. Lu, J.J., Langer, R. & Chen, J. A novel mechanism is involved in cationic lipid-mediated functional siRNA delivery. *Mol. Pharm.* **6**, 763–771 (2009).
39. Varkouhi, A.K., Scholte, M., Storm, G. & Haisma, H.J. Endosomal escape pathways for delivery of biologicals. *J. Control. Release* **151**, 220–228 (2011).
40. Vieira, O., Botelho, R. & Grinstein, S. Phagosome maturation: Aging gracefully. *Biochem. J.* **366**, 689–704 (2002).
41. Rettig, G.R. & Behlke, M.A. Progress toward *in-vivo* use of siRNAs-II. *Mol. Ther.* **20**, 483–512 (2012).
42. Nguyen, J. & Szoka, F.C. Nucleic acid delivery: The missing pieces of the puzzle? *Acc. Chem. Res.* **45**, 1153–1162 (2012).
43. Nechaev, S. *et al.* Intracellular processing of immunostimulatory CpG–siRNA: Toll-like receptor 9 facilitates siRNA dicing and endosomal escape. *J. Control. Release* **170**, 307–315 (2013).
44. Vivero-Escoto, J.L., Slowing, I.I., Trewyn, B.G. & Lin, V.S.-Y. Mesoporous silica nanoparticles for intracellular controlled drug delivery. *Small* **6**, 1952–1967 (2010).
45. Herd, H. *et al.* Nanoparticle geometry and surface orientation influence mode of cellular uptake. *ACS Nano* **7**, 1961–1973 (2013).
46. Rasband, W. ImageJ. U.S. National Institutes of Health. Retrieved from http://imagej.nih.gov/ij/
47. Platt, N., Suzuki, H., Kurihara, Y., Kodama, T. & Gordon, S. Role for the class A macrophage scavenger receptor in the phagocytosis of apoptotic thymocytes *in vitro*. *Proc. Natl. Acad. Sci. U.S.A.* **93**, 12456–12460 (1996).
48. Akinc, A. *et al.* A combinatorial library of lipid-like materials for delivery of RNAi therapeutics. *Nat. Biotechnol.* **26**, 561–569 (2008).
49. Soutschek, J. *et al.* Therapeutic silencing of an endogenous gene by systemic administration of modified siRNAs. *Nature* **432**, 173–178 (2004).
50. Ulvila, J. *et al.* Double-stranded RNA is internalized by scavenger receptor-mediated endocytosis in *Drosophila* S2 cells. *J. Biol. Chem.* **281**, 14370–14375 (2006).
51. Sahay, G. *et al.* Efficiency of siRNA delivery by lipid nanoparticles is limited by endocytic recycling. *Nat. Biotechnol.* **31**, 653–658 (2013).
52. Schroeder, A., Levins, C.G., Cortez, C., Langer, R. & Anderson, D.G. Lipid-based nanotherapeutics for siRNA delivery. *J. Intern. Med.* **267**, 9–21 (2010).
53. Inoue, Y. *et al.* Efficient delivery of siRNA using dendritic poly(l-lysine) for loss-of-function analysis. *J. Control. Release* **126**, 59–66 (2008).
54. Breunig, M. *et al.* Mechanistic investigation of poly(ethylene imine)-based siRNA delivery: Disulfide bonds boost intracellular release of the cargo. *J. Control. Release* **130**, 57–63 (2008).
55. McNaughton, B.R., Cronican, J.J., Thompson, D.B. & Liu, D.R. Mammalian cell penetration, siRNA transfection, and DNA transfection by supercharged proteins. *Proc. Natl. Acad. Sci. U.S.A.* **106**, 6111–6116 (2009).
56. Engels, J.W. Gene silencing by chemically modified siRNAs. *Nat. Biotechnol.* **30**, 302–307 (2013).

57. Stephen, S.L. *et al.* Scavenger receptors and their potential as therapeutic targets in the treatment of cardiovascular disease. *Int. J. Hypertens.* **2010**, 1–21 (2010).
58. Jones, N.L. & Willingham, M.C. Modified LDLs are internalized by macrophages in part via macropinocytosis. *Anat. Rec.* **255**, 57–68 (1999).
59. Canton, J., Neculai, D. & Grinstein, S. Scavenger receptors in homeostasis and immunity. *Nat. Rev. Immunol.* **13**, 621–634 (2013).
60. Murshid, A., Gong, J., Prince, T., Borges, T.J. & Calderwood, S.K. Scavenger receptor SREC-I mediated entry of TLR4 into lipid microdomains and triggered inflammatory cytokine release in RAW 264.7 cells upon LPS activation. *PLoS One* **10**, e0122529 (2015).
61. Miller, D.K. Cell killing by lysosomotropic detergents. *J. Cell Biol.* **97**, 1841–1851 (1983).
62. Huang, H.W., Chen, F.-Y. & Lee, M.-T. Molecular mechanism of peptide-induced pores in membranes. *Phys. Rev. Lett.* **92**, 198304 (2004).
63. Stalder, L. *et al.*, The rough endoplasmatic reticulum is a central nucleation site of siRNA-mediated RNA silencing. *EMBO J.* **32**, 1115–1127 (2013).

SUPPLEMENTARY INFORMATION

Supplementary Table 1 Materials list.

- Four-Well Confocal Plate (LabTek, #155383)
- 96-Well Plate (Costar, #3610)
- Acetic Acid (J.T. Baker, #15500760)
- Ammonium Hydroxide (Sigma, #320145-500ML)
- APTES: (3-Aminopropyl) triethoxysilane (Sigma, #A3648-100ML)
- Chlorpromazine hydrochloride (Sigma, #C8138-5G)
- Copper Grids, 200 Mesh (Electron Microscopy Sciences, #G200-Cu)
- Cytochalasin D (Sigma, #C2618-200 µL)
- DAPI: (4′,6-Diamidino-2-phenylindole dihydrochloride) (Sigma, #10236276001)
- Dextran Sulfate, Mw 500 k (Sigma, #D6001)
- Dextran, Mw 10 k (Sigma, #D9260-10G)
- DMEM (Life Technologies, #11965092)
- DPBS: Dulbecco's NaCl/Pi (Life Technologies, #14040133)
- Ethanol (VWR, #89125-164)
- Fetal Bovine Serum (Life Technologies, #16000044)
- Filipin Complex III (Sigma, #F4767-1MG)
- Formaldehyde/Glutaraldehyde, 2.5% each in 0.1M Sodium Cacodylate Buffer, pH 7.4 (Electron Microscopy Sciences, #15949)
- Formvar Solution in Ethylene Dichloride (Electron Microscopy Sciences, #RT 15820)
- Geneticin (Life Technologies, #10131-035)
- Heparin (Sigma, #H3393-25KU)
- Lead Citrate (Electron Microscopy Sciences, #512-26-5)
- Lipofectamine 2000 (Life Technologies, #11668019)
- Milli-Q Water, 18 MΩ (Millipore, #QTUM000IX)
- Opti-MEM (Life Technologies, #11058021)
- Osmium Tetroxide, 1% (Electron Microscopy Sciences, #19152)
- pDNA (pd2EGFP-N1, clontech #6009-1)
- Penicillin/Streptomycin (Life Technologies, #15140122)
- Round-Bottom Tubes, 5 ml (BD Falcon, #352063)
- siRNA: Sense 5′-GCUGACCCUGAAGUUCAUC-3′; Antisense 5′-GAUGAACUUCAGGGUCAGC-3′ (Dharmacon)
- Fluorescent siRNA: Sense DY547-5′-GCUGACCCUGAAGUUCAUC-3′; Antisense 5′-GAUGAACUUCAGGGUCAGC-3′ (Dharmacon)
- Sodium Cacodylate Buffer (Electron Microscopy Sciences, #11653)
- Sphero Rainbow Calibration Particles (Spherotech)
- Spurr Resin (Electron Microscopy Sciences, #14300)
- SYBR gold staining (Life Technologies, #S-11494)
- TEOS: Tetraethyl Orthosilicate (Sigma, #86578-250ML)
- Trypsin (Life Technologies, #25200056)
- Ultracel Regenerated Cellulose Membrane, 30 kDa NMWL, 47 mm (Millipore, #PLTK04710)
- Uranyl Acetate (Electron Microscopy Sciences, #22400)

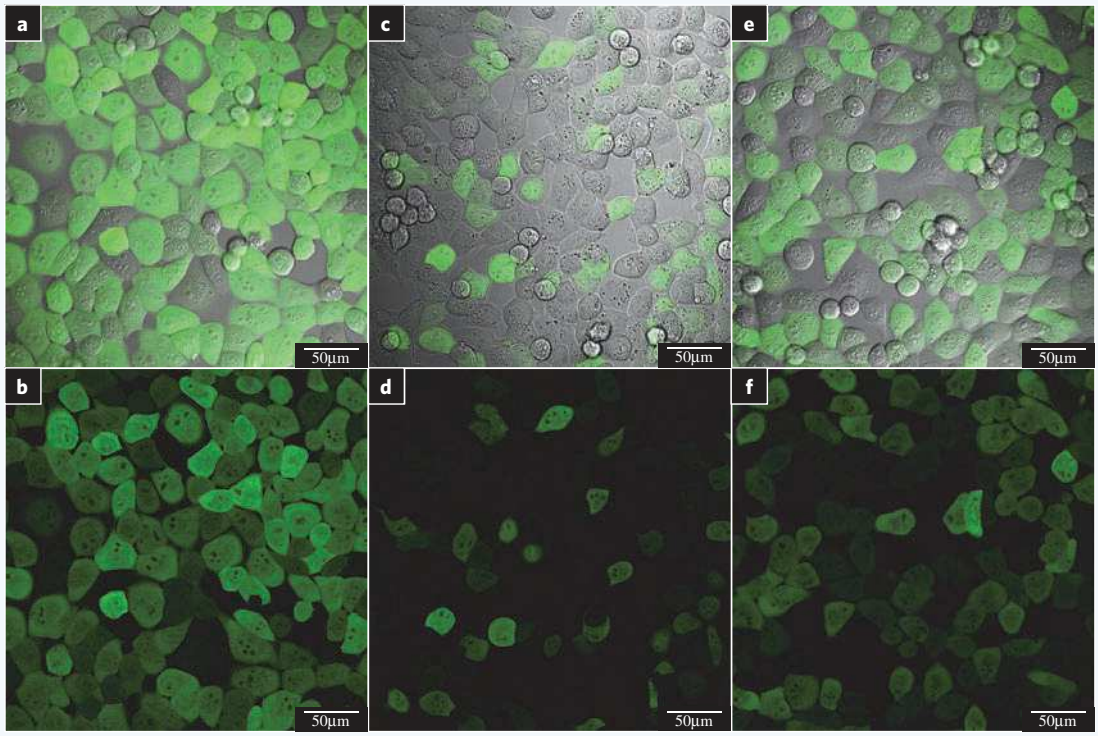

Supplementary Figure 1 Confocal microscopy of delivery vehicle mediated silencing. Confocal images of various siRNA-vehicle complexes 24 hours post-transfection into EGFP-expressing H1299 cells. Green fluorescence represents the EGFP-expressing cells. Gray scale images were obtained from a phase contrast objective. (**a,b**) Control cells with no delivery vehicle. (**c,d**) 2.3 μg/mL of LF2K and 100 nM siRNA. (**e,f**) 200 μg/mL of 40% APTES + Dextran and 100 nM siRNA. Scale bars are 50 μm.

Supplementary Table 2 Statistical analysis for **Supplementary Fig. 2**. Analyses were performed using two-way ANOVA, followed by Tukey's HSD post-hoc analysis in Origin 8. DF, degrees of freedom; sig flag, significance flag, where 0 indicates no significance ($p > 0.05$) level and 1 indicates significance ($p < 0.05$).

		Control (EGFP Fluorescence)					LF2K (EGFP Fluorescence)					40% APTES + Dextran (EGFP Fluorescence)				
		DF	|t| value	P-value	Alpha	Sig flag	DF	|t| value	P-value	Alpha	Sig flag	DF	|t| value	P-value	Alpha	Sig flag
No Inhibitor	Clathrin (Chlorpromazine)	6	0.779	0.943	0.05	0	6	0.132	1.000	0.05	0	6	1.803	0.608	0.05	0
	Caveolae (Filipin)	6	0.255	0.998	0.05	0	6	1.849	0.591	0.05	0	6	0.514	0.982	0.05	0
	Scavenger Receptors (Dextran Sulfate)	6	0.092	1.000	0.05	0	6	7.586	0.007	0.05	1	6	10.049	0.002	0.05	1

		No Inhibitor (EGFP Fluorescence)					Clathrin-Chlorpromazine (EGFP Fluorescence)				
		DF	|t| value	P-value	Alpha	Sig flag	DF	|t| value	P-value	Alpha	Sig flag
Control	LF2K	6	8.141	0.003	0.05	1	6	7.230	0.005	0.05	1
LF2K	40% APTES + Dextran	6	10.997	0.001	0.05	1	6	12.021	3.56E-04	0.05	1
		6	2.856	0.188	0.05	0	6	4.791	0.034	0.05	1

		Caveolae-Filipin (EGFP Fluorescence)					Scavenger Receptors-Dextran Sulfate (EGFP Fluorescence)				
		DF	|t| value	P-value	Alpha	Sig flag	DF	|t| value	P-value	Alpha	Sig flag
Control	LF2K	6	6.548	0.009	0.05	1	6	0.647	0.893	0.05	0
LF2K	40% APTES + Dextran	6	10.738	0.001	0.05	1	6	1.039	0.753	0.05	0
		6	4.191	0.057	0.05	0	6	0.393	0.959	0.05	0

Supplementary Table 3 Statistical analysis for **Fig. 2,3**. Analyses were performed using two-way ANOVA, followed by Tukey's HSD post-hoc analysis in Origin 8. DF, degrees of freedom; sig flag, significance flag, where 0 indicates no significance ($p > 0.05$) level and 1 indicates significance ($p < 0.05$).

		Control (EGFP Fluorescence)					LF2K (EGFP Fluorescence)					40% APFES + Dextran (EGFP Fluorescence)				
		DF	|t| value	P-value	Alpha	Sig flag	DF	|t| value	P-value	Alpha	Sig flag	DF	|t| value	P-value	Alpha	Sig flag
No Inhibitor	Clathrin (Chlorpromazine)	12	1.466	0.940	0.05	0	12	0.022	1.000	0.05	0	12	0.800	0.997	0.05	0
	Caveolae (Filipin)	12	0.436	1.000	0.05	0	12	0.485	1.000	0.05	0	12	1.060	0.988	0.05	0
	Clathrin and Caveolae	12	0.344	1.000	0.05	0	12	1.000	0.990	0.05	0	12	1.778	0.864	0.05	0
	Actin (Cytochalasin D)	12	0.495	1.000	0.05	0	12	4.427	0.091	0.05	0	12	8.033	1.36E-04	0.05	1
	Active Delivery (4°C)	12	0.503	1.000	0.05	0	12	12.688	1.77E-05	0.05	1	12	10.040	4.56E-06	0.05	1
	Scavenger Receptors (Dextran Sulfate)	12	0.238	1.000	0.05	0	12	16.762	8.09E-07	0.05	1	12	14.404	0.00E+0	0.05	1

		Control (siRNA Uptake)					LF2K (siRNA Uptake)					40% APTES + Dextran (siRNA Uptake)				
		DF	|t| value	P-value	Alpha	Sig flag	DF	|t| value	P-value	Alpha	Sig flag	DF	|t| value	P-value	Alpha	Sig flag
No Inhibitor	Clathrin (Chlorpromazine)	12	21.701	2.80E-07	0.05	1	12	1.096	0.985	0.05	0	12	10.264	0.000	0.05	1
	Caveolae (Filipin)	12	0.053	1.000	0.05	0	12	1.446	0.944	0.05	0	12	1.665	0.896	0.05	0
	Clathrin and Caveolae	12	19.995	1.55E-07	0.05	1	12	2.309	0.664	0.05	1	12	11.449	0.000	0.05	1
	Actin (Cytochalasin D)	12	3.870	0.170	0.05	0	12	1.258	0.971	0.05	0	12	13.141	0.000	0.05	1
	Active Delivery (4°C)	12	25.724	1.15E-07	0.05	1	12	3.403	0.239	0.05	1	12	37.931	0.000	0.05	1
	Scavenger Receptors (Dextran Sulfate)	12	6.048	0.014	0.05	1	12	2.836	0.437	0.05	1	12	36.914	0.000	0.05	1

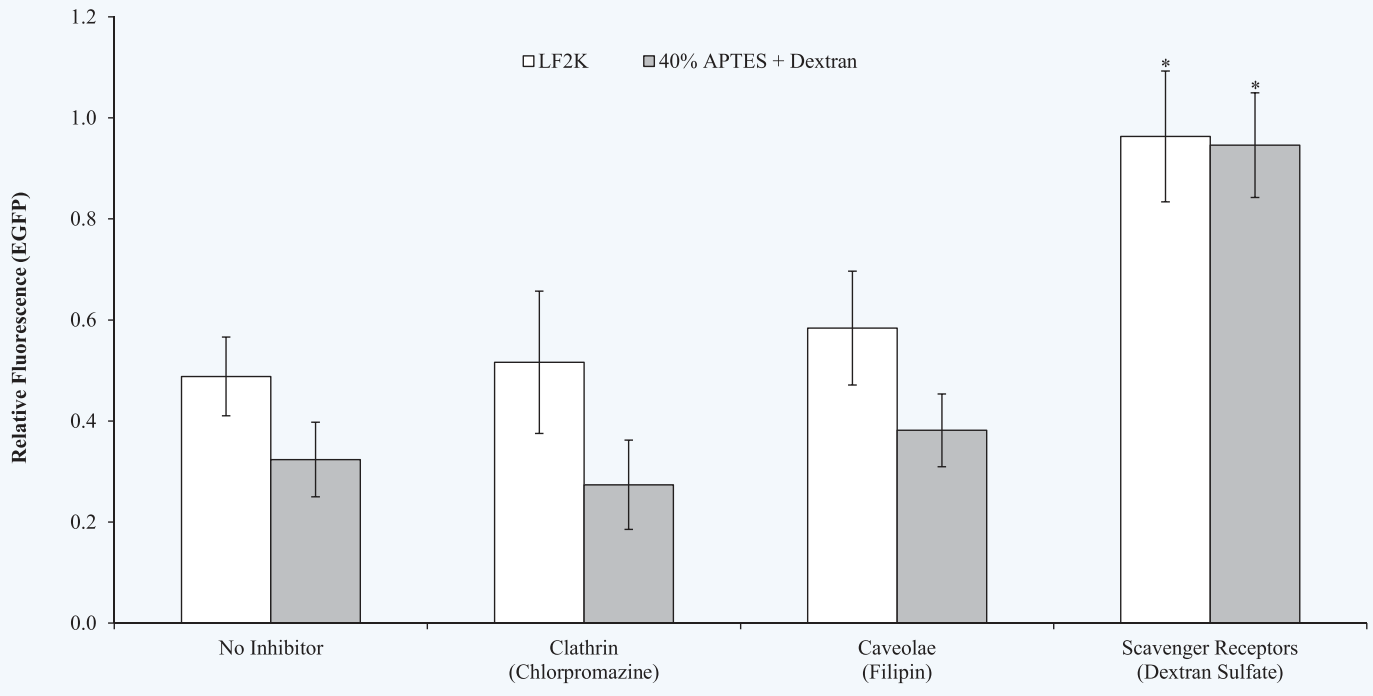

Supplementary Figure 2 EGFP silencing in the presence of endocytotic inhibitors. Relative fluorescence of EGFP-expressing HeLa cells transfected with siRNA complexes. Cells were pre-treated with endocytosis inhibitors and assayed 24 hours post-transfection by flow cytometry. Results were normalized to particle-only controls within corresponding inhibitors. Error bars represent ±1 standard deviation; $n = 3$. Statistical analysis was performed using two-way ANOVA, followed by Tukey's HSD post-hoc analysis. *Significant difference ($p < 0.05$) as compared to conditions without inhibitors.

Supplementary Table 4 Statistical analysis for **Fig. 6**. Analyses were performed using two-way ANOVA, followed by Tukey's HSD post-hoc analysis in Origin 8. Sig flag, significance flag, where 0 indicates no significance ($p > 0.05$) level and 1 indicates significance ($p < 0.05$).

		siRNA Binding (Relative Intensity)					siRNA Degradation (Relative Intensity)				
		q value	Alpha	Sig flag	F value	P-value	q value	Alpha	Sig flag	F value	P-value
Acidic Conditions (pH 4.75)	Neutral Conditions (pH 7.00)	102.532	0.05	1	5256.463	0.00216	2.778	0.05	0	3.859	0.121

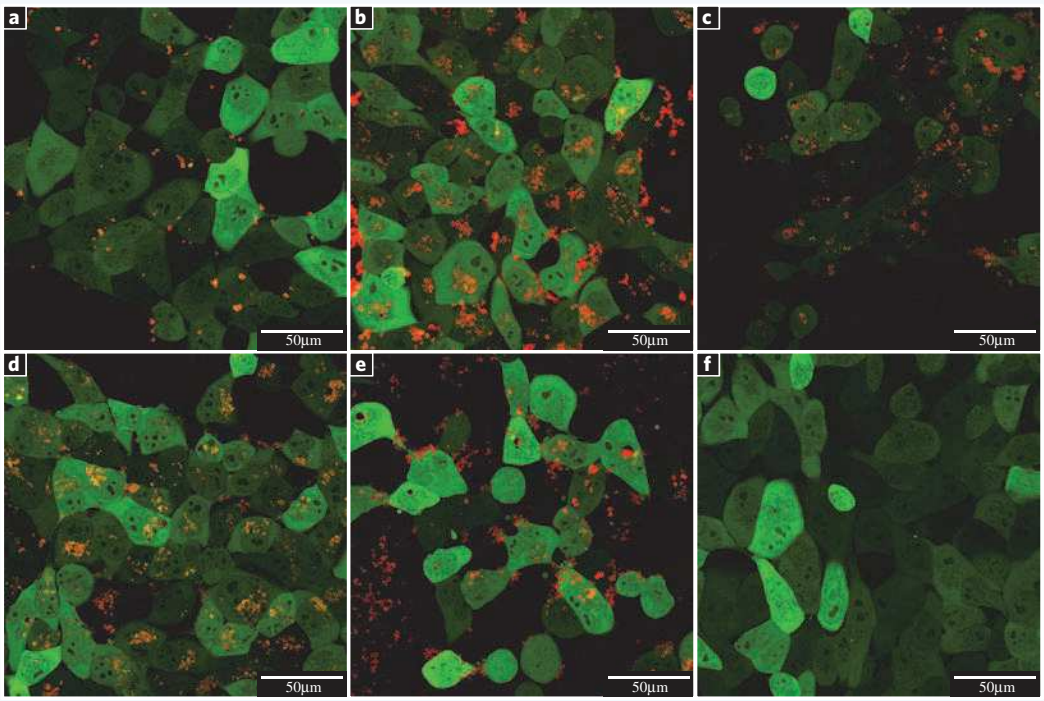

Supplementary Figure 3 Confocal microscopy of delivery vehicle mediated silencing. Confocal images of EGFP-expressing H1299 cells (green) using 100 nM fluorescently labeled siRNA (red) and either (**a**) 2.3 µg/ml LF2K or (**b**–**f**) 200 µg/ml of 40% APTES + Dextran SNP. Images (**c**–**f**) were pre-treated with endocytosis inhibitors and imaged 4 hours post-transfection. Inhibited pathway (inhibitor): (**c**) clathrin (chlorpromazine), (**d**) caveolae (filipin), (**e**) actin (cytochalasin D) and (**f**) scavenger receptors (dextran sulfate).

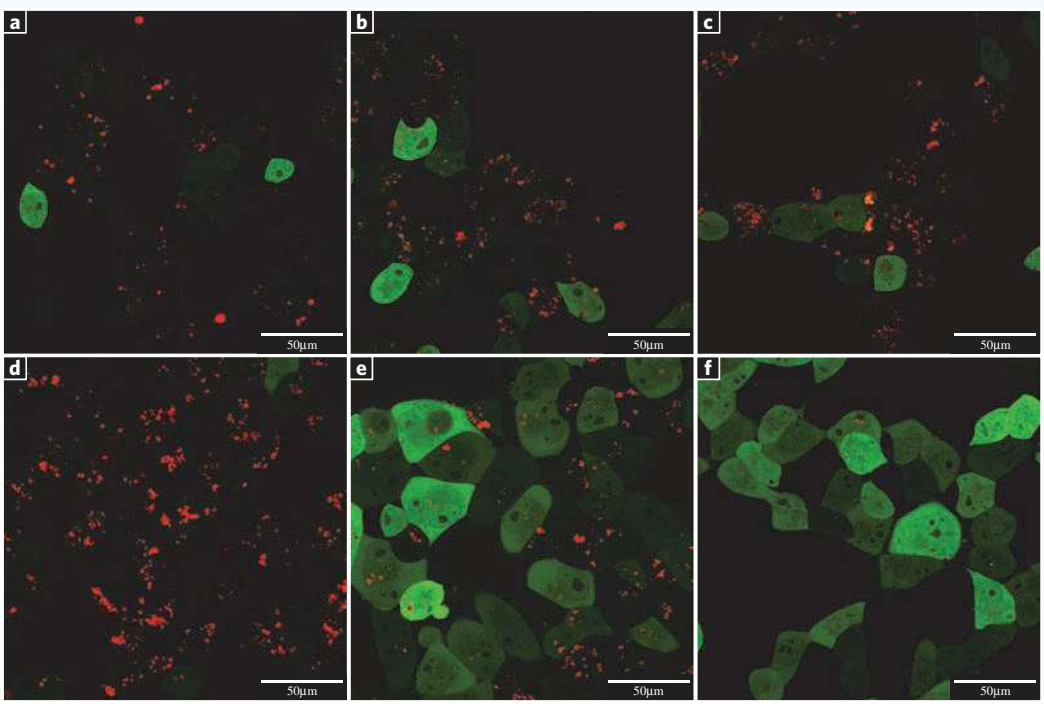

Supplementary Figure 4 Confocal microscopy of delivery vehicle mediated silencing. Confocal images of EGFP-expressing H1299 cells (green) using 100 nM fluorescently labeled siRNA (red) and either (**a**) 2.3 µg/mL LF2K or (**b**–**f**) 200 µg/mL of 40% APTES + Dextran SNP. Images (**c**–**f**) were pre-treated with endocytosis inhibitors and imaged 24 hours post-transfection. Inhibited pathway (inhibitor): (**c**) clathrin (chlorpromazine), (**d**) caveolae (filipin), (**e**) actin (cytochalasin D) and (**f**) scavenger receptors (dextran sulfate).

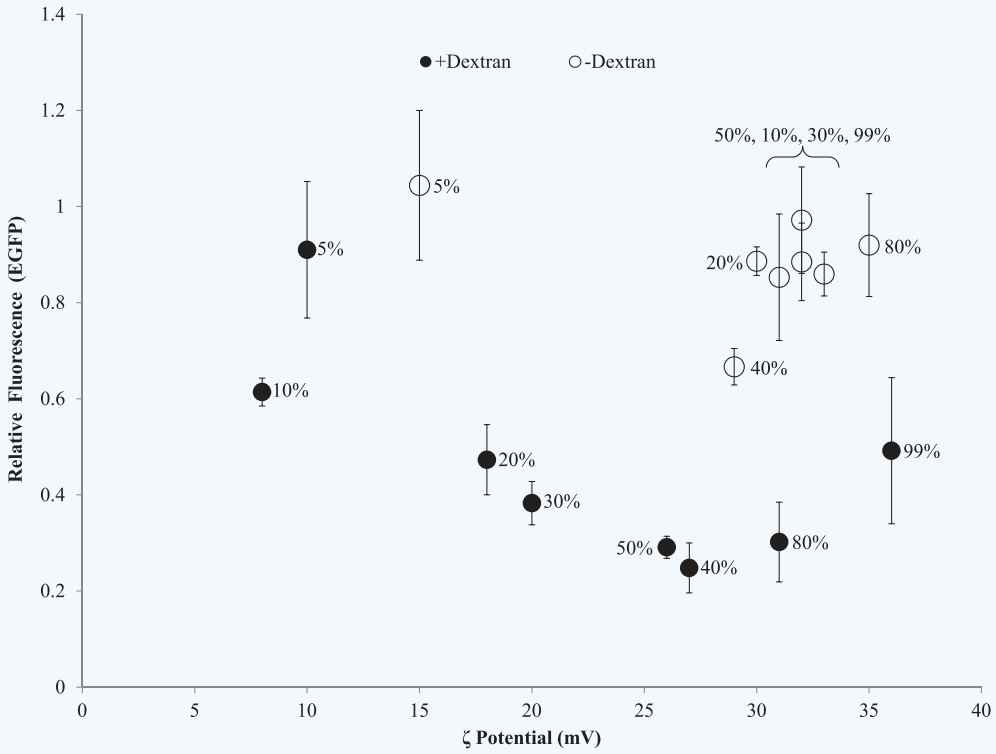

Supplementary Figure 5 Role of SNP zeta potential (mV) on silencing. Zeta potentials were determined using 1 mg/mL of SNPs in HEPES buffer. SNPs were functionalized with varying percentages of APTES and either 0 mol% (hatched) or 1 mol% Dextran (filled). Results were correlated to silencing of the siRNAs after SNP delivery (**Fig. 1**). SNPs containing 0.05% APTES + Dextran (−40 mV) and 0.05% APTES − Dextran (−20 mV) are not shown for clarity of the plot.

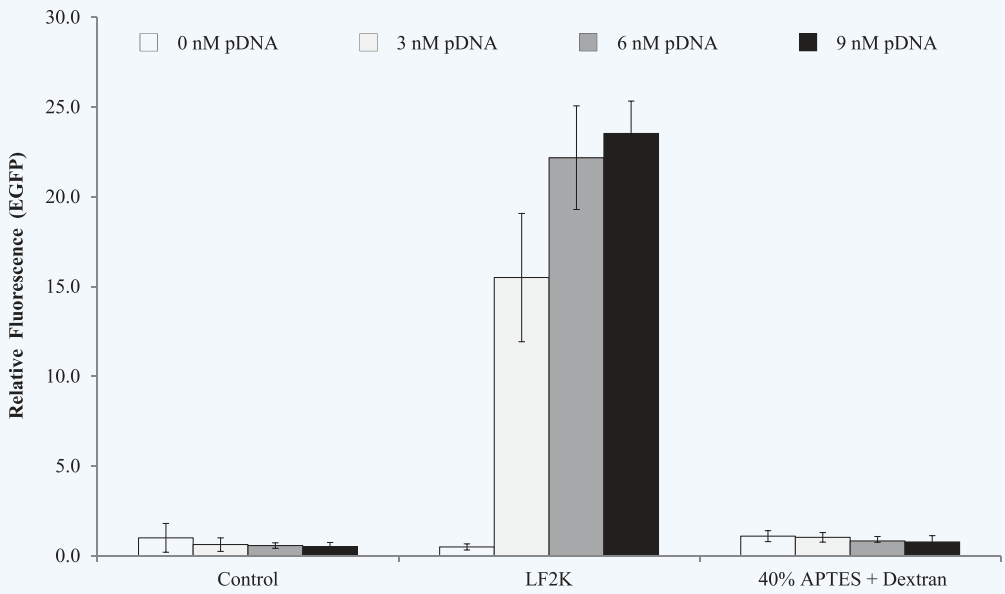

Supplementary Figure 6 Plasmid transfection efficiency of SNPs. The relative fluorescence of EGFP in HeLa cells 24 hours post-transfection with pd2EGFP-N1 vehicle complexes. Results are normalized to the EGFP fluorescence of vehicle-only control cells at 0 nM pDNA. The complexes contain either 2.3 μg/mL of LF2K or 200 μg/mL of 40% APTES + Dextran SNP, and 0, 3, 6 or 9 nM of pDNA. Error bars represent ± 1 standard deviation; $n = 3$.